Synchronized family dynamics in globally coupled maps

N. J. Balmforth
Scripps Institution of Oceanography, University of California, La Jolla, California 92093 and Istituto di Cosmogeofisica, C. Fiume 4, 10133 Torino, Italy

A. Jacobson
Department of Meteorology, Penn State University, 503 Walker Building, University Park, Pennsylvania 16802

A. Provenzale
Istituto di Cosmogeofisica, C. Fiume 4, 10133 Torino, Italy

(Received 5 November 1998; accepted for publication 11 May 1999)

The dynamics of a globally coupled, logistic map lattice is explored over a parameter plane consisting of the coupling strength, ϵ, and the map parameter, a. By considering simple periodic orbits of relatively small lattices, and then an extensive set of initial-value calculations, the phenomenology of solutions over the parameter plane is broadly classified. The lattice possesses many stable solutions, except for sufficiently large coupling strengths, where the lattice elements always synchronize, and for small map parameter, where only simple fixed points are found. For smaller ϵ and larger a, there is a portion of the parameter plane in which chaotic, asynchronous lattices are found. Over much of the parameter plane, lattices converge to states in which the maps are partitioned into a number of synchronized families. The dynamics and stability of two-family states (solutions partitioned into two families) are explored in detail. © *1999 American Institute of Physics.* [S1054-1500(99)01503-7]

In nonlinear dynamics, one of the ways to construct rich, complicated systems is by coupling a large number of low-order dynamical systems. These extensive systems can then be used as metaphors for physical situations in which our ability to explore fully a particular natural phenomenon is limited by the complexity of the dynamics. In this article we study an example of such a coupled system: a lattice of logistic maps that are globally coupled through a mean field. As we show, the coupling of the maps creates a system with a rich variety of different behaviors, and the overall wealth of behavior becomes overwhelming. We explore some aspects of these riches, such as ''synchronization'' and ''clustering.'' For strong coupling between the maps, global synchronization takes over, and the whole system behaves as a single logistic map. At values of the coupling strength below the synchronization threshold, the system displays partial or ''family'' synchronization (clusters), coexisting attractors, and complicated bifurcation sequences.

I. INTRODUCTION

The dynamics of coupled, mutually interacting chaotic systems is extremely rich, and can display properties which are not detectable in the behavior of the individual elements. Among the simplest of such systems are coupled map lattices, composed of an ensemble of low-dimensional maps whose evolution is determined by both their own dynamics and the dynamics of the other elements of the ensemble.[1,2] Lattice coupling schemes may either be *local* or *global*. For local coupling, each map interacts only with its nearest neighbors. In a global coupling scheme, however, the evolution of each map is affected by the dynamics of all other maps. Sites on a locally coupled lattice have a spatial meaning, and a larger distance of two maps on the lattice implies a weaker interaction between them.

On the other hand, if the evolution of any map of a globally coupled system is equally affected by the state of all of the other maps, then one can hardly interpret the lattice in terms of spatial distributions, and proximity of two maps on lattice sites does not convey any particular meaning. Indeed, the description of the system as a ''lattice'' is a little misleading. Rather, these globally coupled systems must be seen as an ensemble of individual elements, each of which equally communicates with all the others, and are amenable to analysis in terms of mean field theory. For example, one application of globally coupled map lattices that is frequently mentioned is to arrays of Josephson junctions.[3]

In this paper, we consider a system of globally coupled logistic maps, and study its dynamics as a function of both the value of the individual map parameter and the coupling strength. For strong coupling, the map lattice synchronizes and all maps have the same value at the same time, behaving as a single logistic map. Just below the synchronization threshold, individual maps can sporadically leave the synchronized state in a process which is reminiscent of on–off intermittency.[4,5] Well below the synchronization threshold, however, new types of behavior are present.

For example, Weisenfeld and Hadley[3] observed a multiplicity of coexistent stable solutions in coupled circle maps. They found a large number [order of $(N-1)!$, where N is the number of elements in the system] of stable periodic orbits within such a system, and remarked on how stochastic perturbations may induce the system to jump from one basin of attraction to another. They called this phenomenon ''at-

tractor crowding.'' Subsequently, Kaneko[6,7] reported finding similar results in a globally coupled logistic map lattice.

In addition, Kaneko found a rich variety of what we call ''family''-synchronized solutions. These are global attractors for which the N maps are partitioned into k groups with N_k members in each. Each of these groups is a ''family,'' and within each family all the maps are synchronized to one another. The term ''clustering'' has also been used in the literature to describe these types of solutions, but we avoid this terminology here because it suggests the importance of spatial proximity, which is not the case.

The possible relevance of family synchronization in biological networks has been considered in Ref. 8. Family synchronization can be observed also for continuous time dynamical systems, as discussed in Refs. 3, 9, and 10 for globally coupled oscillators and in Ref. 11 for coupled chaotic systems. A weaker form of synchronization in chaotic systems, called phase synchronization, has been studied in Ref. 12.

In the following, after formulating the problem in Sec. II, we define synchrony and asynchrony in coupled map lattices (Sec. III), and we discuss the coexistence of many periodic attractors at low values of the coupling strength in Sec. IV. Section V reports an extensive set of initial-value calculations, from which we draw a picture of the system behavior in parameter space. Section VI is devoted to a detailed study of the dynamics of two-family solutions and Sec. VII gives conclusions and perspectives.

II. FORMULATION

The system of interest in this study is a lattice of N globally coupled, one-dimensional maps. The lattice evolution is described by

$$x_{n+1}(j)=(1-\epsilon)f[x_n(j)]+\frac{\epsilon}{N}\sum_{k=1}^{N} f[x_n(k)], \tag{1}$$

where j and k are indices of maps within the lattice, n and $n+1$ are successive moments in discrete time [hence $x_n(i)$ is the nth iteration of the ith map in the lattice], the coupling strength is measured by the parameter ϵ, and $f(x)$ is the function describing the dynamics of the individual maps.

The coupled map system can be written in the alternative form,

$$x_{n+1}(j)=(1-\epsilon)f[x_n(j)]+\epsilon M_n, \tag{2}$$

where

$$M_n=\frac{1}{N}\sum_{j=1}^{N} f[x_n(j)] \tag{3}$$

is the *mean field*. The coupling strength ϵ varies between zero (the uncoupled limit) and unity (complete coupling; each map evolves only according to the mean field).

All the lattices discussed in this study are constructed using logistic maps, for which

$$f(x_n)=1-ax_n^2, \tag{4}$$

where a is a parameter. (This is, strictly speaking, the quadratic map, rather than the logistic map, but the two are identical up to a simple change of variable.) This map has the property that any initial condition on the interval $[-1, 1]$ will remain on that interval under the action of the map, provided $a<2$.

III. SYNCHRONY AND ASYNCHRONY

Our system has two parameters, a and ϵ. Though the behavior of the system over the (ϵ,a) parameter plane is very complicated, there are two special cases in which the dynamics is relatively straightforward and well understood.

The first case is when the lattice is completely uncoupled $(\epsilon=0)$. In this limit, each map evolves independently of all the others and the dynamics of each of the uncoupled elements is simply that of the logistic map. In other words, the state of the system is always *asynchronous*, unless the initial condition of each element is identical, or if, for some reason, the maps eventually all converge to the same orbit. The bifurcation sequence of the logistic map is a canonical example in dynamical systems theory. Three important values of the map parameter are:

(i) $a=a_2=0.75$: first period doubling,
(ii) $a=a_4=1.25$: second period doubling,
(iii) $a=a_\infty\approx 1.4$: accumulation point of the period-doubling cascade.

The other special limit is $\epsilon\to 1$. In this case, the elements see only the mean field and so evolve identically. In other words, from any initial condition, the elements immediately *synchronize*. Again, the subsequent evolution is dictated by a single logistic map.

Independent of the value of ϵ, it is also straightforward to show that if $x_1(j)=X_1$ for every j, then $x_n(j)=X_n$ for all n, and $X_{n+1}=1-aX_n^2$. That is, the synchronized state is an invariant manifold of the system for all parameter values. However, the individual elements can be chaotic, in which case, for $\epsilon=0$, initially close elements diverge from one another exponentially quickly. Hence, we expect that this synchronized state is unstable for sufficiently small ϵ, where the sensitivity to initial condition overcomes the tendency to synchronize.

The stability threshold $\epsilon=\epsilon_c(a)$ can be computed by linearizing about the synchronized orbit of the system: Let

$$x_n(j)=X_n+\xi_n(j), \tag{5}$$

where $|\xi_n(j)|\ll 1$. Then,

$$\xi_{n+1}(j)=(1-\epsilon)f'(X_n)\xi_n(j)+\epsilon m_n, \tag{6}$$

where

$$m_n=\frac{1}{N}f'(X_n)\sum_{k=1}^{N}\xi_n(k) \tag{7}$$

is the perturbation to the mean field.

There is a solution to (6) that is of the form, $\xi_n(j)=\Xi_n$ for all j. The solution satisfies $\Xi_{n+1}=f'(X_n)\Xi_n$, which gives a stability exponent that is just the Lyapunov exponent of the logistic map, $\lambda(a)$. This solution corresponds to a *synchronized* perturbation because $\xi_n(j)$ is independent of j. Hence, the stability exponent characterizes per-

turbations inside the invariant synchronization manifold, which is why we recover the logistic map's Lyapunov exponent.

The remainder of the solutions to (6) can be taken to be of the separable form,

$$\xi_n(j) = A_n e(j), \tag{8}$$

with the property $m_n = 0$, or

$$\sum_{j=1}^{N} e(j) = 0 \tag{9}$$

(of which there are $N-1$ independent solutions). Hence the orientation of the vector **e** does not change and the amplitudes evolve according to

$$A_{n+1} = (1-\epsilon) f'(X_n) A_n . \tag{10}$$

The associated stability exponents therefore have an $(N-1)$-fold multiplicity and all are equal to

$$\Lambda(a) = \ln(1-\epsilon) + \lambda(a). \tag{11}$$

These solutions are perturbations away from the synchronization manifold, so $\Lambda(a)$ denotes a transverse stability exponent. Hence, if $(1-\epsilon)\exp\lambda(a) > 1$, that state is unstable. Thus, the stability threshold is given by

$$\epsilon = \epsilon_c(a) = 1 - e^{-\lambda(a)} \tag{12}$$

(Kaneko;[7] Ding and Yang[5]), which is drawn in Fig. 1. In fact, Fig. 1 displays much more than this threshold; it encapsulates many of our results and is essentially our point of summary. In the sections to follow, we build up the results portrayed in Fig. 1.

Note that, $\epsilon_c \leqslant 0$ if the Lyapunov exponent is null or negative. Thus, only chaotic synchronized solutions, or periodic states that are unstable within the synchronization manifold itself [both with $\lambda(a) > 0$], can be *transversely* unstable.

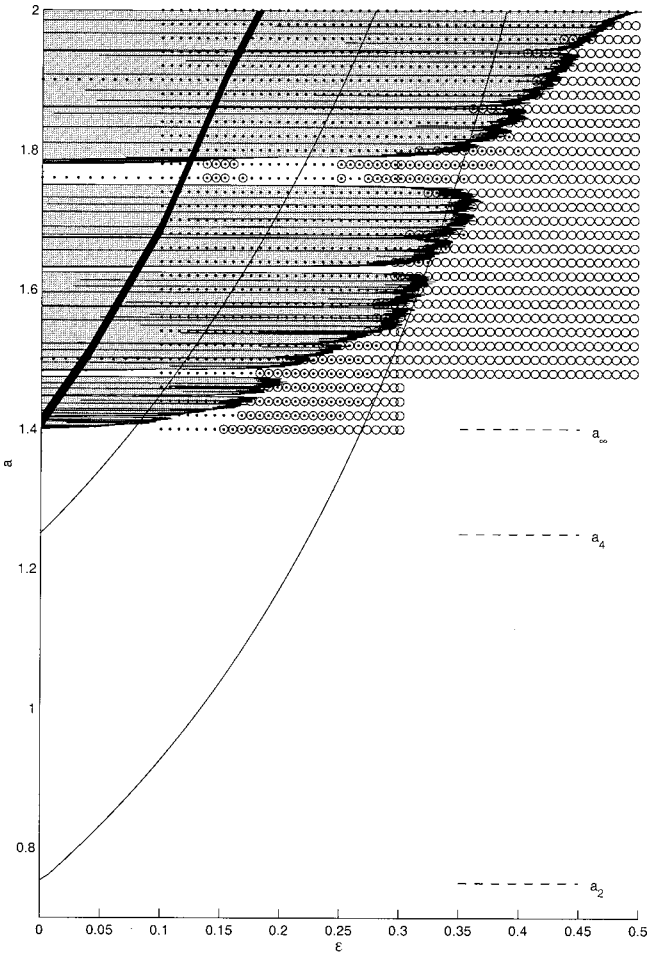

FIG. 1. The area shaded in darker gray is the region in which the synchronized state is unstable. The area shaded in lighter gray is the region over which there is a stable, asynchronous, period-two orbit in which the elements of the system are equally partitioned into two families (which requires N even). The dots show parameter values at which initial-value calculations converged to states that were not fully synchronized. The circles show initial-value calculations in which fully synchronized states were observed. For lower values of a and larger values of ϵ, synchronization is inevitable. The thick solid line approximately locates the desynchronization ''cliff,'' where synchronized families largely cease to emerge in initial-value computations and completely desynchronized solutions become rife.

IV. SIMPLE PERIODIC SOLUTIONS

For $a < a_\infty$, the logistic map has a stable, periodic orbit. Hence, if there is no coupling, the individual map elements always converge to that orbit. Moreover, a finite coupling strength does not prevent the elements converging to this same orbit provided the initial conditions are not too far apart. This is essentially the reason why synchronized states are always stable whenever the logistic map has a stable periodic orbit [in this instance, $\lambda(a) < 0$ and so $\epsilon_c(a) < 0$]. Nevertheless, these stable, synchronized periodic orbits are not the only states to which the system can converge, and in this section we indicate how one uncovers the full range of possibilities. The technique is essentially the same as the method of continuation from the anti-integrable limit used in discrete nonlinear field theories.[13]

The synchronized solutions are characterized by each element of the lattice converging to identical points or phases of the stable periodic orbit. However, for a stable period-2^p orbit, there are 2^p distinct points on the orbit and so there are correspondingly many possible phases of the cycle to which each element of the lattice could converge, if uncoupled. Thus, at $\epsilon = 0$, in addition to the perfectly synchronized solutions, there is a whole multitude of other orbits in which the elements oscillate out of phase with one another. Moreover, these asynchronous states are all stable because the period-2^p orbit is stable. Hence, by continuity, we expect that these solutions all remain stable for sufficiently small ϵ.

For sufficiently large coupling, however, only the fully synchronized solution persists. Thus there must be bifurcations in which the asynchronous solutions eventually disappear. To uncover these bifurcations we can trace the solutions to larger ϵ from the weakly coupled limit. However, there are further bifurcations that occur which can destabilize these solutions before they ultimately disappear; these secondary bifurcations involve some other, unstable solutions.

The unstable solutions can be constructed in the same fashion as the asynchronous stable states: At $\epsilon = 0$, not only is there a stable period-2^p orbit, but there are two unstable fixed points and a set of unstable periodic orbits with periods 2^q, $q = 1, \ldots, p-1$. Of these, we safely may ignore one of the

TABLE I. Combinations of initial conditions for a two-map lattice in the period-2 window from which we may construct all the independent periodic solutions (barring combinations that include the other unstable fixed point with $x<0$ which always lies outside the attractor).

Condition	Map 1	Map 2	
1	X_1	X_1	Stable, synchronized
2	X_1	X_f	Unstable
3	X_1	X_2	Stable
4	X_f	X_f	Unstable, synchronized

fixed points (the point lying in $x<0$) since that point always lies outside the range of values of x covered by the attractors of the system, if $a<2$. (It is straightforward to show that if the initial conditions of the map all lie inside the interval $[-1, 1]$, then once the system has converged to an attractor, the most negative value for $x_{n+1}(j)$ over all possible $x_n(j)$ is $1-a$, which is always above the negative fixed point, $x=[-\sqrt{1+4a}-1]/(2a)$, unless $a\geqslant 2$.) But there is another multitude of unstable periodic orbits for the uncoupled map lattice in which one or more of the elements execute one of these unstable trajectories.

A. Period-2 window: $a_2<a<a_4$

We illustrate the variety of periodic equilibria with $a_2<a<a_4$, so there is a stable period-2 solution of the logistic map, $X_2=f(X_1)$ and $X_1=f(X_2)$. At $\epsilon=0$, there are therefore two possible, stable synchronized states with $x_n(j)=X_1$ or $x_n(j)=X_2$, $j=1,...,N$. There is, in addition, a variety of stable asynchronous states in which some number, say M, of the maps converge to one phase of the period-2 orbit, $X_1\rightarrow X_2\rightarrow X_1\ldots$, and the others ($N-M$ in number) converge to the other phase, $X_2\rightarrow X_1\rightarrow X_2\ldots$. There is also an unstable synchronized state: $x_n(j)=X_f$, where $X_f\equiv[\sqrt{1+4a}-1]/(2a)$ is the (relevant) unstable fixed point, and a variety of unstable asynchronized solutions in which one, or more, of the elements lies at X_f, and the others execute some phase of the period-2 orbit.

For $N=2$, the total number of equilibria can be generated from the combinations listed in Table I. From master combinations like these, we can construct all the possible equilibrium states at a certain value for a, then continue them to higher ϵ to uncover the bifurcations exhibited by the system. We do this numerically using Newton's method; the stability of the states can be found as a biproduct of the iteration scheme.

In Fig. 2, we see the results of tracing the possible branches for $a=1.2$ (which is inside the window of stable period-2 orbits), and lattices with $N=2$, 4, 5, and 10. The solid horizontal line at the top and bottom of the pictures represent stable, fully synchronized states, in which all maps are oscillating in phase. The horizontal dashed line in the center of the plot represents the unstable, synchronized state. The other, curved branches are the asynchronous solutions. The stable asynchronous solutions all loose stability in various secondary bifurcations that take the form of either subcritical pitchforks or saddle nodes. For example, at $\epsilon\approx 0.21$ in Fig. 2(a), there is a subcritical pitchfork bifurcation in which two solutions corresponding to line 4 of Table I destabilize the stable, asynchronous solution obtained from line 3.

Ultimately, the remaining unstable branches (of which there are $N-1$ in number) end in a highly degenerate, period-doubling bifurcation at X_f [$\epsilon\approx 0.285$ in Fig. 2(a)]. This degenerate bifurcation occurs when the transverse stability exponent of the unstable synchronized state, with multiplicity $N-1$ and derived in Sec. III, passes through zero. That is, for $\epsilon=1-\epsilon^{-\lambda_f}$, where $\lambda_f=\ln(2aX_f)\equiv\ln[\sqrt{1+4a}-1]$ is the stability exponent of the unstable fixed point.

The diagrams become more and more complicated as N increases. The general trend is for a multitude of stable equilibria near $\epsilon=0$, that gradually disappear on raising ϵ, leaving only synchronized solutions. In other words, the bifurcation diagrams parallel (and, of course, underlie) some of the features present in Fig. 1. But, Fig. 1 fails to convey the wealth of possible solutions existing at small coupling, which is apparent even for low N in Fig. 2. This multiplicity is equivalent to the ''attractor crowding'' of Weisenfeld and Hadley.[3]

B. Period-4 window: $a_4<a<a_8$

We repeat the computation of the bifurcation diagrams for $a=1.3$, which lies inside the window in which there is a stable period-4 orbit of the logistic map. In this case there are many more possible equilibrium states at small ϵ; these states develop as shown in the bifurcation diagrams of Fig. 3. Suffice to say that there are more branches and more bifurcations.

Roughly speaking, these period-4 diagrams have smaller structures inside them that are much like the bifurcation diagrams pictured above [e.g., the region $0<\epsilon<0.2$ and $-0.3<x<0$ is rather like Fig. 2(b), but with extra branches]. That similarity probably extends beyond the period-4 case, so that there are pieces of the period-2^p bifurcation diagram that resemble the period-2^{p-1} diagram, and there must be an interesting self-similarity to the bifurcation diagram at the accumulation point of the period-doubling cascade ($a=a_\infty$).

Another feature of the bifurcation sequence is revealed in Fig. 3(a). The asynchronous, period-2 solution with partition 2:2 is evident in this figure as the curve that ends for $\epsilon\approx 0.325$ at the unstable fixed point, $X_f\approx 0.57$. The period-2 solution is unstable at $\epsilon=0$, but a bifurcation stabilizes this branch at $\epsilon\approx 0.0277$, and it remains stable up to $\epsilon\approx 0.24$. The first change of stability is through a Hopf bifurcation (cf. Ref. 14), and a stable two-loop attractor exists for lower ϵ which is not drawn on the diagram. At still lower ϵ, these loops disappear by colliding with some of the period-4 orbits. The secondary bifurcations of these loopy attractors become very complicated for $a>a_\infty$, and will be considered further in Sec. VI C.

The 2:2 asynchronous period-2 solution describes a lattice that is equally partitioned into two synchronized families. That is, it is an example of one of Kaneko's family-synchronized solutions. Indeed, because of the form of the mean field, this particular state is also a solution for all lattices of arbitrary, even N. On the general lattice, the state is one of equal partition, so that $N/2$ maps execute one orbit, and the other $N/2$ maps are synchronized to another trajec-

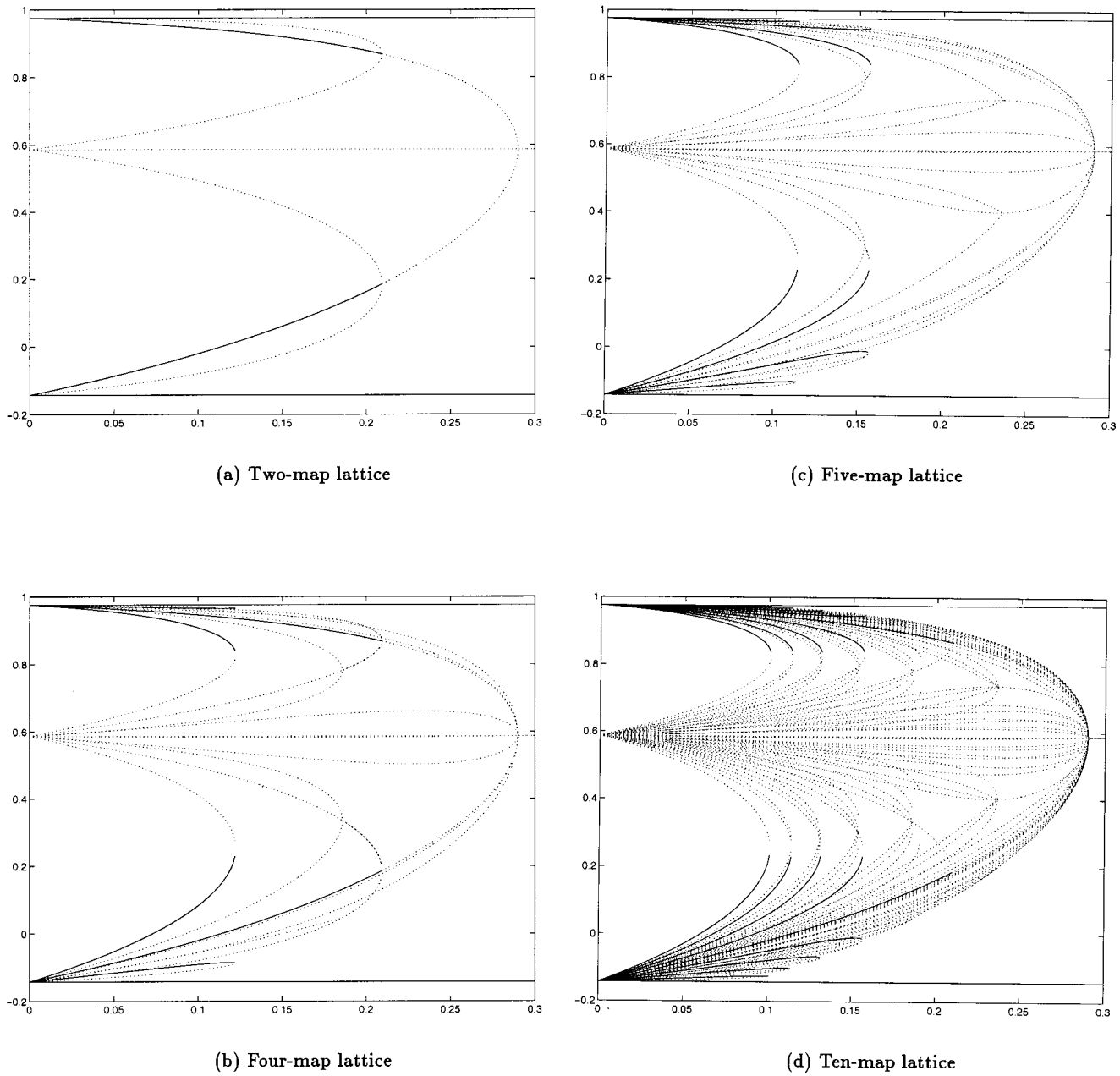

FIG. 2. Bifurcation diagrams for lattices of varying size when the map parameter $a=1.2$ is in the period-two window. Stable solutions are depicted with a solid line, unstable solutions with a dotted line. In all cases, the bifurcation parameter is coupling strength, ϵ, and the values $x_n(j)$ are plotted.

tory. Note that the state remains stable over a range in ϵ for values of a that lie well into the chaotic regime. This band, for $N=2$, is shown as the region shaded in lighter gray in Fig. 1 (the left-hand boundary of this band denotes the Hopf bifurcation that generates loopy attractors). However, by using the techniques described in Sec. VI A, we verify that the state is also stable within this band on lattices of arbitrary (even) N. This illustrates how solutions that are partitioned into synchronized families occur over wide regions of the parameter plane, a feature of the lattice dynamics that is explored further in Sec. V by solving initial-value problems.

V. INITIAL-VALUE CALCULATIONS

The study outlined in Sec. IV reveals a plethora of coexisting, periodic equilibria for $a<a_\infty$, but it says nothing of what happens when the map parameter enters the regime in which the logistic map is chaotic. To gain a rough idea of the kinds of attractors that exist for $a>a_\infty$, we performed an extensive set of initial-value calculations with various values for a and ϵ taken from a grid covering this part of the parameter plane (the grid is represented in Fig. 1). Early on in this enterprise we realized that this computation exposed a wealth of different types of attractors and there was no simple transition between synchronization at larger coupling strengths and asynchronization in the weak-coupling limit; we basically opened Pandora's box. Because of this wealth of possibilities we have opted primarily for a relatively crude description based on the phenomenology of states that partition themselves into synchronized families; that is, family-synchronized solutions. The example we focused on at the

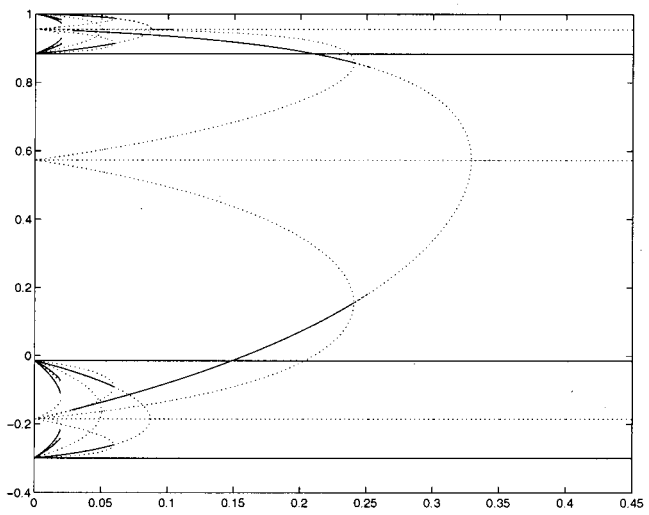

(a) Two-map lattice

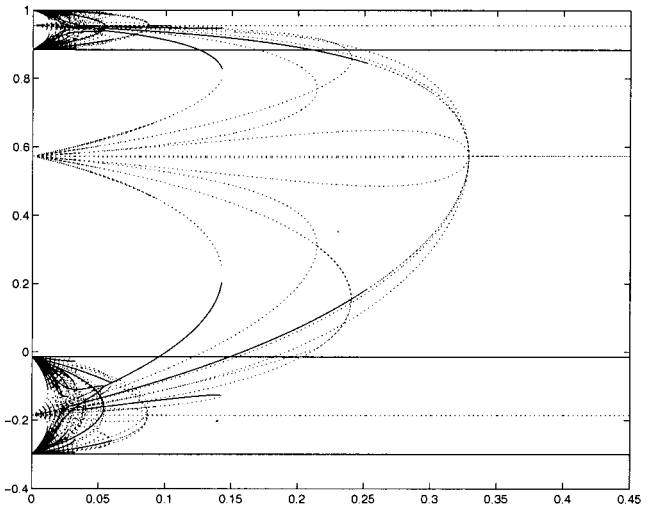

(b) Four-map lattice

FIG. 3. As in Fig. 2, but for map parameter $a=1.3$ (in the period-four window).

end of Sec. IV contained two families, but more generally there may be K partitions, with $K<N$, leading to ''K-family solutions.''

An example of an initial-value calculations for $N=100$, $\epsilon=0.385$, and $a=1.9$ is shown in Fig. 4. This figure shows two features of the dynamics that were commonly encountered in the initial-value problems. First, the path to the attractor is typically rather tortuous, with the system passing through extensive periods of asynchronous irregularity and ephemeral regular states (see Fig. 4; such behavior was previously noticed by Kaneko,[6,7] and makes the identification of attractors rather involved). Second, the attractor (which appears at the top of Fig. 4) is a family-synchronized solution with a small number of partitions (in this case, $K=2$).

In fact, for these particular parameter values, we find that randomly initialized lattices fall almost exclusively into one of three categories of two-family attractors. If we denote the number of elements in the smaller family by M, then these three two-family states are characterized by

(1) $M=10$ or $\alpha=0.1$; period-3,
(2) $M=9$ or $\alpha=0.09$; period-3,
(3) $M=8$ or $\alpha=0.08$; chaotic,

where $\alpha=M/N$ (this label uniquely classifies solutions in lattices with varying N). The attractor of Fig. 4 is of type 1.

Figure 5 shows another example, this time of type 3. This attractor is not periodic; if we plot $x_{n+3}(j)$ against $x_n(j)$ for the larger family, we arrive at the picture shown on the left-hand side of Fig. 5. A closer inspection of the object in the picture reveals what appears to be an underlying fractal structure. Moreover, in form, the object is very similar to an attractor of the Hénon map. This suggests that the solution is chaotic and has a dimension between one and two.

In fact, the similarity of the two-family state in Fig. 5 to a Hénon attractor is not so surprising, as we discuss in detail in Sec. VI, such two-family states are exactly described by a two-dimensional map. But before we delve into those specifics, we summarize our initial-value computations.

A. A regime diagram

Detailed results of the initial-value calculations are displayed in Fig. 6. This figure shows the number of families in the final attractors over the parameter plane; essentially, it is a regime diagram showing which K-family states are typically found over a range of parameter values. The diagram was created using 50 randomly initialized runs at each of 1570 points in the parameter plane. The map parameter a was varied between 1.4 and 1.98 in steps of 0.02; the coupling strength ϵ was varied from 0.1 to 0.5 in steps of 0.075. There is a rectangular window at $\epsilon>0.3$ and $a<1.42$ for which results were not computed (here, solutions invariably synchronized).

For each run, the lattice was initially iterated 300 000 times. The lattice was then further iterated until a measure of statistical stationarity was achieved, up to a maximum of another 500 000 iterations. The quantity that was monitored for stationarity was the lattice mean,

$$\overline{x_n}=\frac{1}{N}\sum_{j=1}^{n} x_n(j). \tag{13}$$

The first three statistical moments of both a short- and long-term running series of $\overline{x_n}$ were computed. The two series were 75 000 and 300 000 iterations long, respectively. For each moment, the short-term and long-term values were compared. If all three pairs of moments were equivalent to within a certain threshold, the lattice was said to be in a state of statistical stationarity, so that further iteration could be discontinued. One quarter of the runs never met our stationarity criterion after the maximum number of iterations (8×10^5). One explanation of this failure is that transients on the lattice can be exceptionally prolonged; another is that the convergence of statistical averages is very slow. After these iterations, the lattice was tested for partitioning. This check

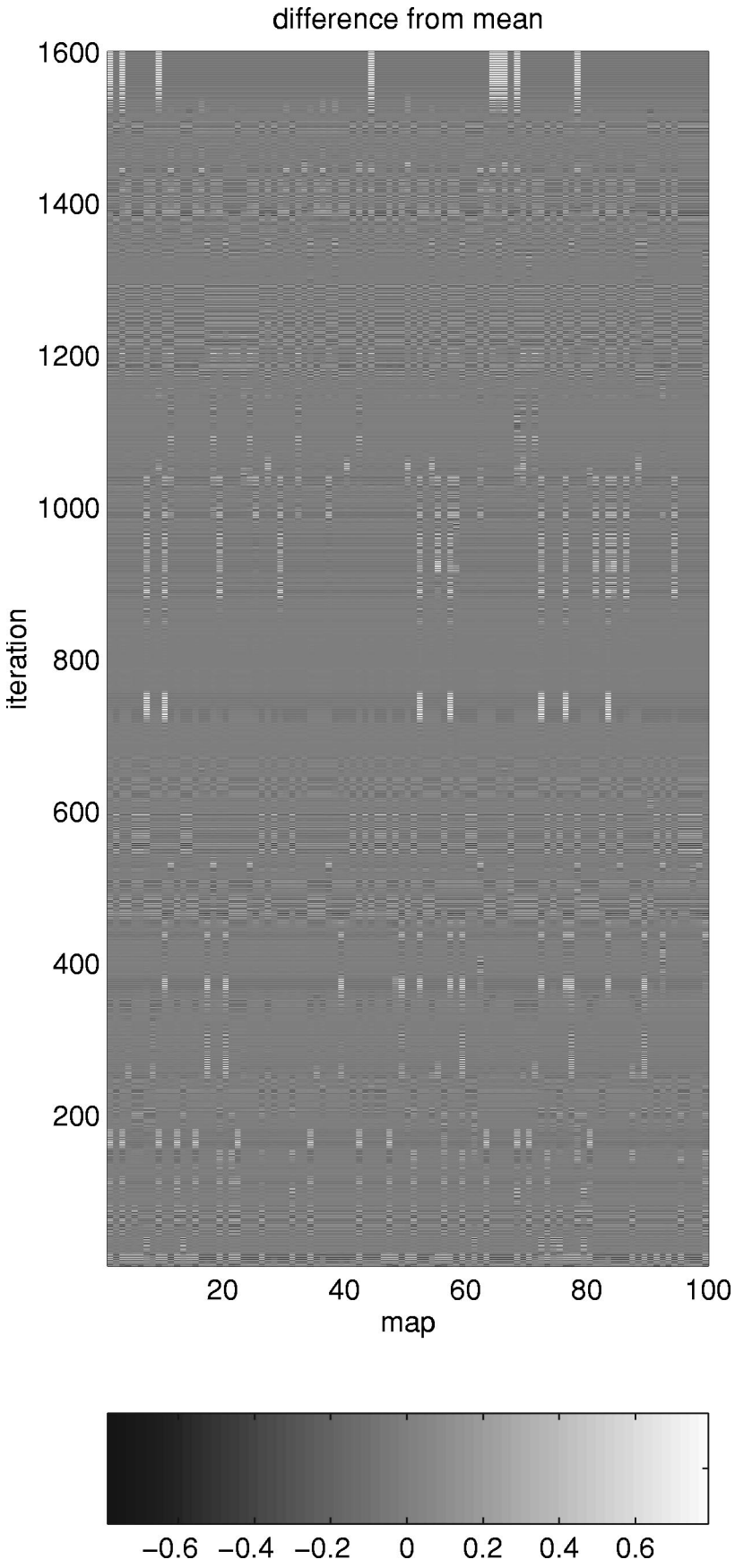

FIG. 4. An initial value problem at $\epsilon=0.385$ and $a=1.9$ for a lattice with $N=100$. The picture shows a diagram of $x_n(j)-\overline{x_n}$, where $\overline{x_n}$ is the lattice mean at the nth instant, plotted on the (j,n) plane, with shading corresponding to level as shown in the key. The diagram chiefly shows a very long transient, but the state to which the system converges at the top of the picture is a two-family attractor in which 10 of the map elements execute identical trajectories, and the other 90 execute another common orbit. By plotting departures from the lattice mean, we highlight ephemeral regular states such as the two-family state with partition $M=7$ that briefly exists near $n=750$, and the nearly synchronized lattice which occurs thereafter (recognizable by featureless gray). Curiously, similar partitioning of the lattice recurs over hundreds of iterations, even though one would imagine that chaos obliterates any past knowledge after only a few iterations. Thus, the lattice possesses a memory of past ephemeral states, suggesting the presence of long temporal correlations (see also Ref. 15).

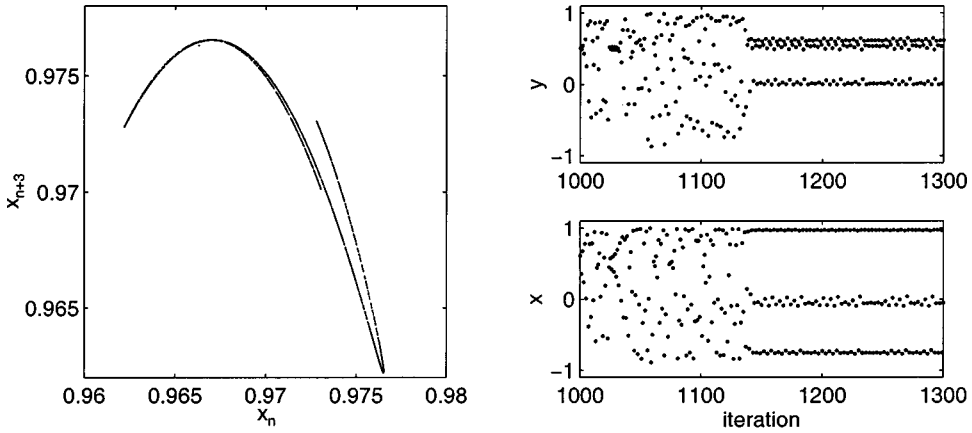

FIG. 5. A second two-family attractor at the same parameter values as Fig. 4. This attractor is chaotic. The larger family has 92 members, and the smaller family has 8. (Left) A plot of x_{n+3} against x_n for the larger family. (Right, top) Time series of map 1, which becomes a member of the smaller family. (Right, bottom) Time series for map 2, a member of the larger family. The members of the smaller family are located haphazardly within the lattice. This is solely a result of the randomly chosen initial conditions; spatial information is, as we already mentioned, not relevant.

was conducted by taking two maps to be in the same family if the cumulative squared difference in map values summed over 1000 more iterations was less than 10^{-6}.

The main feature brought out in Fig. 6 is that over a significant portion of the parameter plane, the system converges to solutions that are either fullly synchronized or partitioned into a small number of families (notably two families). That is, K-family solutions are almost always encountered. Also, there is a distict trend in which K increases with map parameter, but decreases with coupling strength. This leads to the characteristic ''plateaux'' with increasing elevation in Fig. 6.

The lines that define the boundaries of a given plateau (K value) in Fig. 6 generally run diagonally across the $\epsilon-a$ plane [the boundary between one-family and two-family states approximately follows the critical coupling threshold (12); see also Fig. 1]. This reflects a competition between the synchronizing or stabilizing influence of increased coupling,

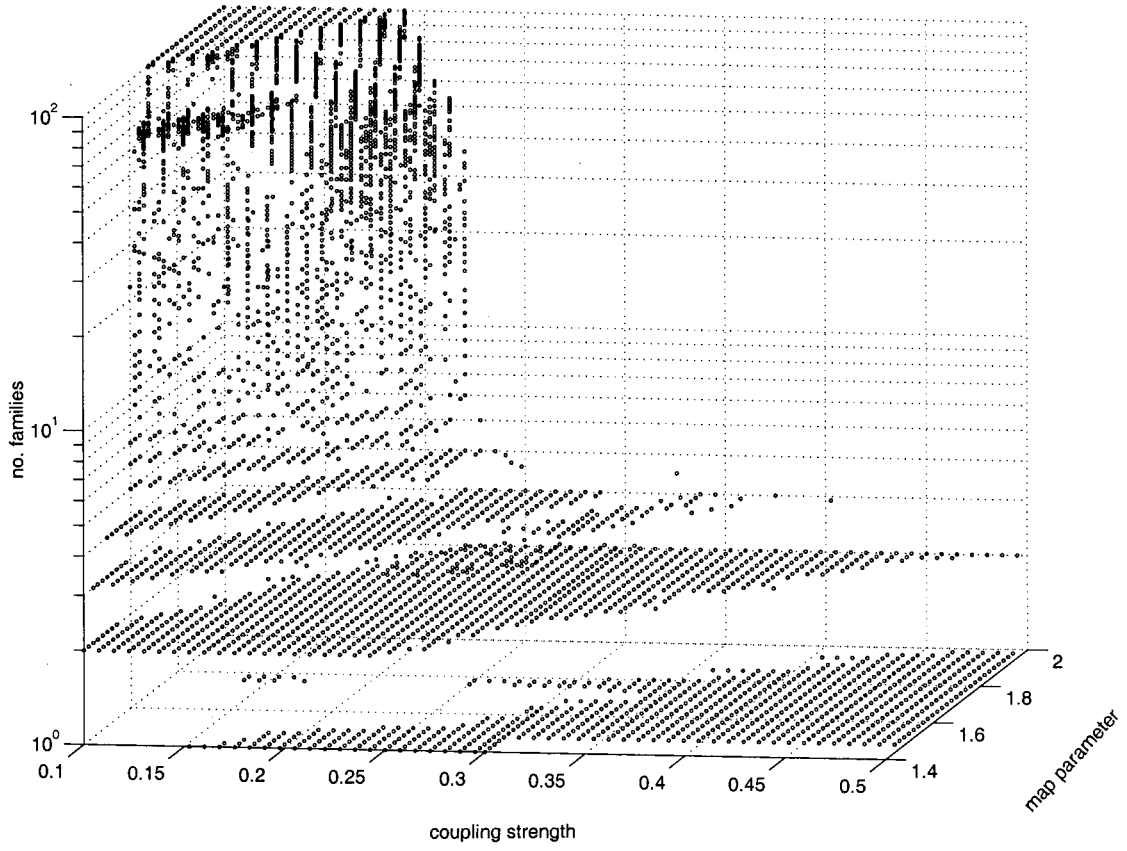

FIG. 6. Number of families in final states plotted as points above the parameter plane. Each dot signifies that some number of the runs at the corresponding a and ϵ values had final states with that number of families. Note that the vertical axis is logarithmic. The methodology is described in the text.

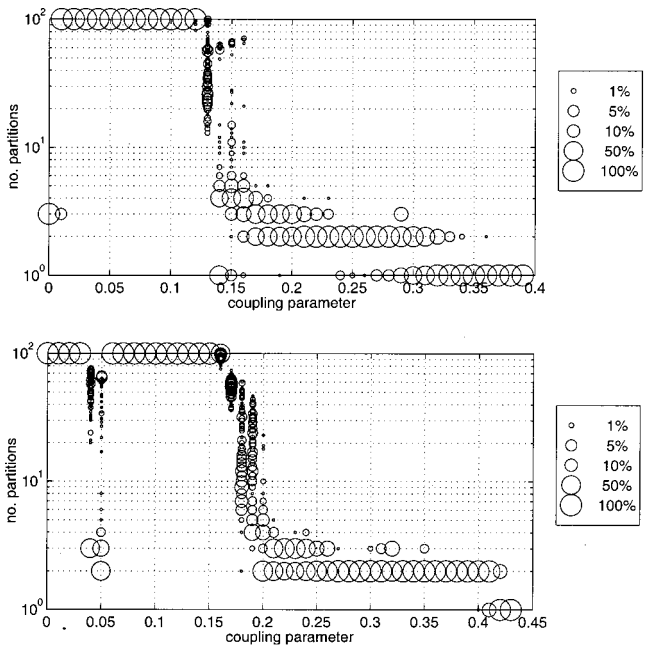

FIG. 7. Slices through the parameter plane of Fig. 6 at (a) $a=1.76$ and (b) $a=1.9$. The size of the symbol, as given by the key, is the percentage of the 200 randomly initialized runs which manifested the given number of families in their final states.

and the destabilizing influence of increased map parameter.

As the K values increase, the ascent up the plateaux steepens dramatically and a ''cliff'' is encountered (the scale of K in Fig. 6 is logarithmic). This is the limit in which we encounter full desynchronization; the rough location of the cliff is also sketched in Fig. 1. Some of the gross features of Fig. 6 were found previously by Kaneko.[6,7]

B. Parameter slices at fixed *a*

A more refined study of the final states can be conducted by considering slices at fixed a or ϵ. Here we examine parameter slices at fixed map parameter. Complementary results for parameter slices at fixed coupling strength are given by Kaneko.[16,17]

Specifically, we consider two representative values of the map parameter: $a=1.76$, and $a=1.9$. For the first case, the logistic map is inside a period-3 window. The second case, $a=1.9$, appears to be exemplary for lattices in which the map parameter gives a chaotic logistic map. For these sections, 200 independent runs with randomly chosen initial conditions were used. The results are shown in Figs. 7–9.

In Fig. 7, the general trend is again revealed for a greater number of families as the coupling strength is reduced. But it is interesting to observe that after the complete desynchronization limit is reached [at $\epsilon\approx 0.14$ in panel (a) and $\epsilon\approx 0.19$ in (b)], there are windows at lower ϵ in which family-synchronized solutions reappear. For $a=1.76$, these states are related to the stable period-3 orbit of the logistic map and emerge near $\epsilon=0$. However, despite the existence of stable synchronization over this entire parameter slice these are not synchronous solutions; such solutions are only encountered with regularity at larger ϵ (the probability of finding a synchronized period-3 orbit at $\epsilon=0$ is easily computed and, though finite, is very small for $N=100$). For $a=1.9$ on the other hand, family-synchronized states re-emerge near $\epsilon=0.05$ where, rather curiously, there is some tendency for a bimodal distribution in partition number, K (solutions with $K=2-4$ and $K=40-50$ are most prevalent).

The rise to complete desynchronization is also not completely unstructured. At $a=1.76$ [panel (a)], there is a peculiar structure to the cliff between $\epsilon=0.13$ and $\epsilon=0.16$, in which some preference for states with $K=30-40$ is shown. Both these features (the occurrence of narrow islands of synchronized families at small ϵ, and the peculiar structures in the cliff) embarass any simple description of the transition to asynchrony.

In Fig. 8 we display some other properties of the family-synchronized states. In particular, we display the partitioning for two- and three-family states over the two parameter slices. For the two-family states we draw $\alpha=M/N$, and for $K=3$, the fraction of map elements in the smallest family; the different symbols denote whether the state was periodic or chaotic.

The two-family states occupy distinct regions in Fig. 8 and the periodic and chaotic solutions are cleanly separated, suggesting simple bifurcation pathways between the two. For example, there is a broad triangular region at higher α where periodic solutions occur; these are chiefly period-2 orbits and their subharmonics. As we lower ϵ these states appear to bifurcate to chaos. There is another group at $a=1.9$ and larger ϵ with small α that are mostly period-3 orbits and their relatives. In this case, the temporal flavor of the dynamics seems most strongly influenced by α. We reproduce the two distributions and describe the implicit bifurcations in Sec. VI, when we consider two-family states explicitly.

The distributions of periodic and chaotic solutions for $K=3$ show more structure than for the two-family states. However, we will not explore this structure in any detail. We only draw the reader's attention to one interesting detail in Fig. 8, which is that the regions in which most of the three-family states are found have an intimate connection with the triangular-shaped area occupied by two-family states. The two regions adjoin one another with almost no overlap. Moreover, the two regions appear to share a common, right-hand border. One explanation of this feature is that the two- and three-family states are different forms of identical attractors. More specifically, as we reduce ϵ, the two-family states in the triangular region gradually undergo a conversion into three-family states. Further details of this fragmentation process are described in Sec. VI C.

Finally, Fig. 9 gives an indication of the frequency of finding chaos along the parameter slices. This picture shows how many of the total number of runs ended in a chaotic state. The ''onset'' of predominant chaos at smaller ϵ (that is, the boundary of the region in which all the runs ended chaotically) roughly coincides with the cliff. To the right, chaos emerges when (and if) chaotic synchronized states predominate.

To complement Fig. 9, in Table II, we compare the number of the K-family states that were periodic to those that were chaotic. This comparison clearly reveals how synchronized-family solutions with a small number of parti-

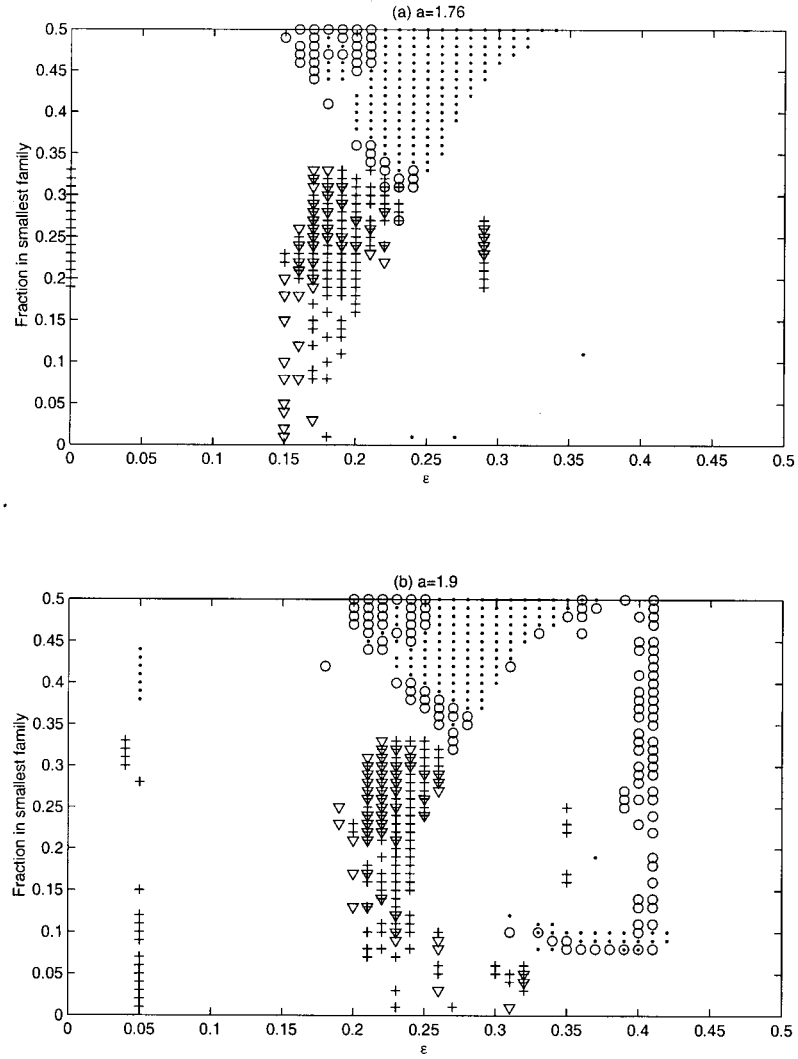

FIG. 8. Partitioning of two- and three-family states with ϵ. Dots indicate periodic solutions, and circles refer to chaotic states for $K=2$. The $K=3$ states are again divided into periodic (+) and chaotic (triangles).

tions are more typically periodic. The property does not remain true as the number of partitions increases, but it is the low K solutions that predominate over extensive portions of the parameter plane.

In other words, for chaotic individual maps, there is a clear tendency that the organization of the lattice into synchronized families reduces the temporal complexity (see also Ref. 18). Thus, global coupling provides a mechanism to

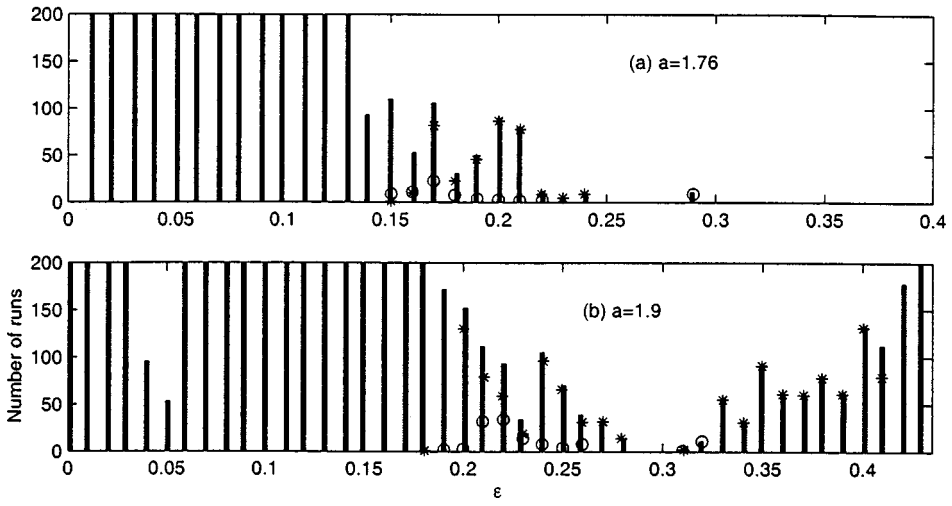

FIG. 9. A histogram of the number of runs that ended in chaotic states. The star indicates the number of chaotic runs that were also two-family states, and the circles show the same for three-family solutions.

TABLE II. Ratios of periodic to chaotic final states for two- and three-family solutions, also for $K=4$ and 5, and for all the states, at the two values of a used for our parameter slices, and also at $a=1.5$.

a	Two-family	Three-family	$K=4$	$K=5$	All states
1.76	1966: 351	670: 78	197:131	28:25	4761:3281
1.9	2665:1184	601:117	63: 41	21: 9	3357:5443
1.5	2202: 252	358: 3	551: 62	121: 2	3421:3579

suppress the chaos in the individual elements, suggesting that, in this case, the whole (the lattice) is less than the sum of the parts (the chaotic logistic maps). However, the converse can also be true: uncoupled maps in stable periodic orbit windows can also become chaotic through coupling [Fig. 9(a)].

VI. TWO-FAMILY DYNAMICS

The initial-value computations reported above illustrate the preponderance of K-family states, and in particular, two-family solutions. When a lattice falls into one of these states, its dynamics is vastly simplified. In particular, the dynamics of a K-family state is described by a K-dimensional map. In this section we focus on the two-family case, but much of what we describe is also true for families with more partitions.

For $K=2$, the elements of the lattice are divided into two partitions. One partition contains M elements and is described by a common variable X_n; the other contains $N-M$ maps and can be represented by Y_n. In this circumstance, the map equations reduce to the two-dimensional system,

$$\begin{aligned} X_{n+1} &= (1-\epsilon) f(X_n) + \epsilon M_n \\ Y_{n+1} &= (1-\epsilon) f(Y_n) + \epsilon M_n , \end{aligned} \tag{14}$$

where the mean field is

$$M_n = \alpha f(X_n) + (1-\alpha) f(Y_n). \tag{15}$$

A. Stability of two-family solutions

The stability of the two-family state in the full map lattice can be found along similar lines to those followed to determine the stability threshold of the fully synchronized solution.

First, we reorganize the lattice so that the first partition consists of maps, $x_n(j)=X_n$, indexed by $1\leqslant j\leqslant M$, and the other partition by maps, $x_n(k+M)=Y_n$, with $1\leqslant k\leqslant N-M$. Then we let

$$\begin{aligned} x_n(j) &= X_n + \xi_n(j) \quad \text{for } j=1,...,M, \\ x_n(k+M) &= Y_n + \eta_n(k) \quad \text{for } k=1,...,N-M, \end{aligned} \tag{16}$$

with $|\xi_n(j)|\ll 1$ and $|\eta_n(k)|\ll 1$.

The perturbations, $\xi_n(j)$ and $\eta_n(k)$, evolve according to

$$\begin{aligned} \xi_{n+1}(j) &= (1-\epsilon) f'(X_n) \xi_n(j) + \epsilon m_n \\ \eta_{n+1}(k) &= (1-\epsilon) f'(Y_n) \eta_n(k) + \epsilon m_n , \end{aligned} \tag{17}$$

where

$$m_n = \alpha f'(X_n) \sum_{j=1}^{M} \xi_n(j) + (1-\alpha) f'(Y_n) \sum_{k=1}^{N-M} \eta_n(k). \tag{18}$$

We construct a perturbation inside the ''two-family manifold'' by taking $\xi_n(j)=\Xi_n$ and $\eta_n(k)=\Upsilon_n$, for every j and k. Then,

$$\begin{aligned} \Xi_{n+1} &= [1-\epsilon(1-\alpha)] f'(X_n) \Xi_n + \epsilon(1-\alpha) f'(Y_n) \Upsilon_n , \\ \Upsilon_{n+1} &= (1-\epsilon\alpha) f'(Y_n) \Upsilon_n + \epsilon\alpha f'(X_n) \Xi_n . \end{aligned} \tag{19}$$

This construction gives the usual Lyapunov exponents for an orbit of the two-dimensional map in (14).

There are two types of perturbations that are transverse to the two-family manifold. These are again solutions that are of separable form: We take either

$$\xi_n(j) = A_n u(j), \quad \eta_n(k) = 0, \tag{20}$$

or

$$\xi_n(j) = 0, \quad \eta_n(k) = B_n v(k), \tag{21}$$

for $j=1,...,M$ and $k=1,...,N-M$, where the vectors $\mathbf{u}$ and $\mathbf{v}$ satisfy

$$\sum_{j=1}^{M} u(j) = 0, \quad \sum_{k=1}^{N-M} v(k) = 0 \tag{22}$$

(with $M-1$ and $N-M-1$ independent solutions, respectively). The first of these perturbations destroys the synchrony of one partition, whereas the second perturbation destroys the other's. Both have the feature that the mean field vanishes and so the orientation of the two perturbations is fixed. We have either

$$A_{n+1} = (1-\epsilon) f'(X_n) A_n$$

or

$$B_{n+1} = (1-\epsilon) f'(Y_n) B_n . \tag{23}$$

Hence the stability exponents for transverse perturbations are

$$\begin{aligned} \Lambda_x &= \ln(1-\epsilon) + \left[\frac{1}{n} \sum_{r=1}^{n} \ln|f'(X_r)| \right]_{n\to\infty} \\ &\equiv \ln[2a(1-\epsilon)] + \left[\frac{1}{n} \sum_{r=1}^{n} \ln|X_r| \right]_{n\to\infty} , \\ \Lambda_y &= \ln(1-\epsilon) + \left[\frac{1}{n} \sum_{r=1}^{n} \ln|f'(Y_r)| \right]_{n\to\infty} \\ &\equiv \ln[2a(1-\epsilon)] + \left[\frac{1}{n} \sum_{r=1}^{n} \ln|Y_r| \right]_{n\to\infty} . \end{aligned} \tag{24}$$

The eigenvalue Λ_x has multiplicity $M-1$, whereas Λ_y is repeated $N-M-1$ times. (This analysis is easily generalized to states with more partitions.)

The forms of the transverse stability exponents are rather elegantly given in terms of mean properties of X_n and Y_n. However, those averages reflect a statistic of the attractor that depends on its detailed structure. For a chaotic attractor,

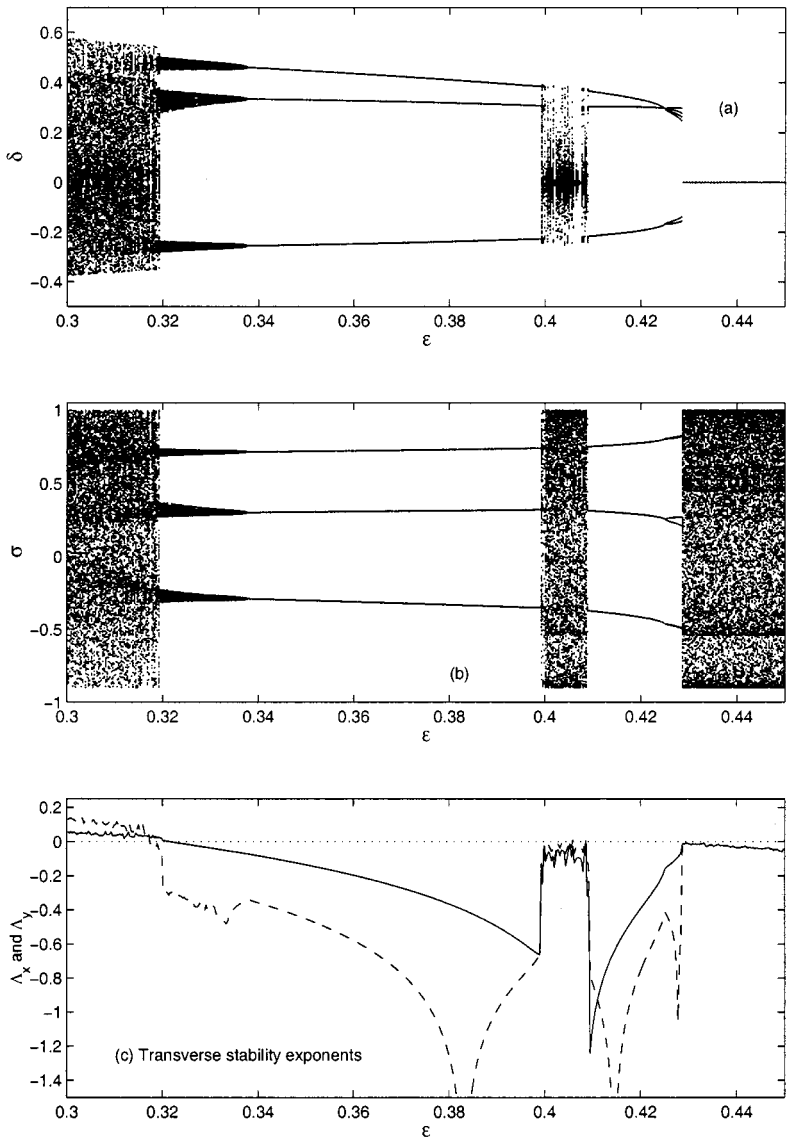

FIG. 10. Bifurcation diagram for the two-family map with $a=1.9$ and $\alpha=0.10$. (a) δ_n, (b) σ_n at different coupling strengths. For each value of ϵ, the two-dimensional map (14) was iterated 5000 times, and the diagrams show the next 200 iterations (there is no attempt to include every attractor should multiple ones exist). In (c) we show the transverse stability exponents, Λ_x and Λ_y.

such a statistic must invariably be computed numerically, and may not even be a simple function of parameters (much like the usual Lyapunov exponent).

B. Two-family bifurcation sequences

To explore the bifurcations of the two-family solution itself, we employ the map (14). This map has three parameters, α, ϵ, and a. In practice, we adopt values for a and α, then vary ϵ. Also, there is little point in full-scale exploration of the bifurcations of every two-family solution of the lattice system, so we opt for a detailed description of a few special cases. These illustrative examples are two-family solutions with $N=100$ and $a=1.9$, which were found as end states in Sec. IV.

The bifurcation diagrams of two particular solutions with $\alpha=M/N=0.1$ and 0.08 are shown in Figs. 10 and 11, respectively. A third case, with equal partitioning ($\alpha=0.5$), is shown in Fig. 12. The first two bifurcation diagrams correspond to solutions displayed in Figs. 4 and 5; they appear in the lower right-hand part of Fig. 8(b). The equal partitioned solution is an example of the kind of solution found in the triangular area shown in Fig. 8(b). The temporal variability (periodic or chaotic) indicated in the bifurcation diagrams coincides with that found in Fig. 8(b).

Displayed in Fig. 10 are values of the quantities, $\delta_n=(X_n-Y_n)/2$ and $\sigma_n=(X_n+Y_n)/2$; only δ_n is shown in the other three bifurcation diagrams. Synchronized solutions have the property $\delta_n=0$, which makes them easy to pick out on these bifurcation diagrams. Also, despite slight differences in the partitions of the families in Figs. 10 and 11, there are significant variations in the bifurcation diagrams (again burdening us with an appreciation of the overcomplicated lattice dynamics).

There are various transitions in Figs. 10–12. Some of these are standard types of bifurcation sequences familiar in one-dimensional maps. However, other transitions are not of the standard variety and are peculiar to higher-dimensional maps. For example, near $\epsilon=0.34$ in Fig. 11 there is a familiar period-doubling cascade (though the cascading orbit begins as period-3 and the attractors look like those of the

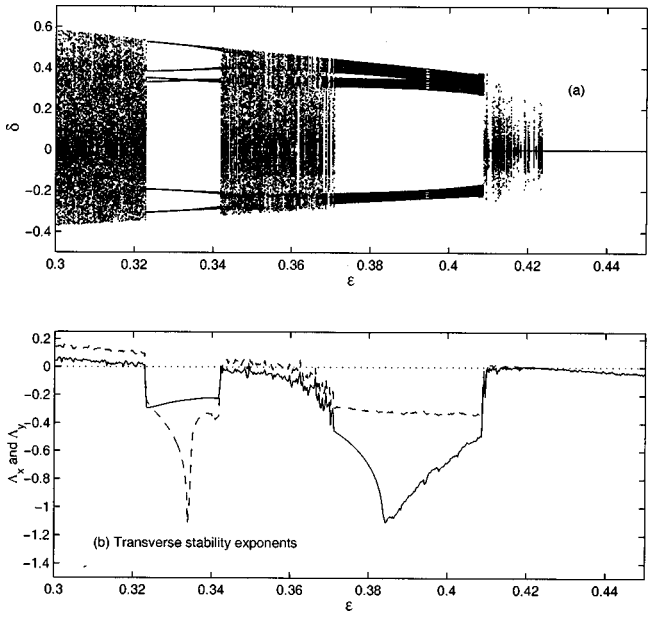

FIG. 11. Bifurcation diagram for the two-family map with $a=1.9$ and $\alpha=0.08$. (a) δ_n, (b) the transverse stability exponents, Λ_x and Λ_y.

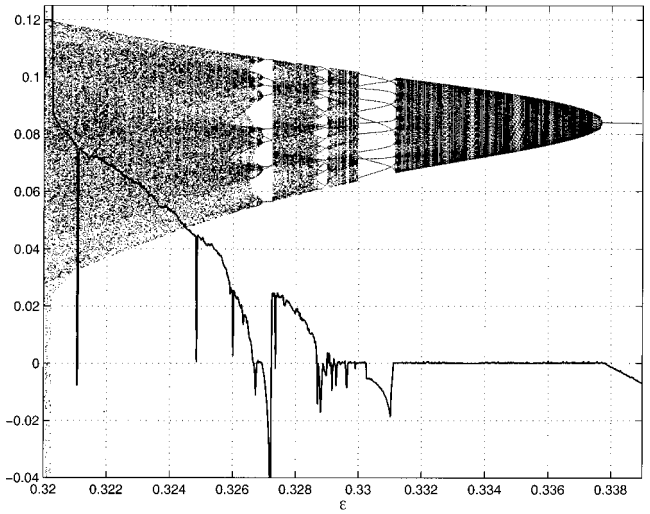

FIG. 13. Leading Lyapunov exponent along the bifurcation sequence also pictured. This sequence is part of the diagram in Fig. 10; shown is $\delta_n - 0.25$ over a range that displays only one part of the three-component attractor. $a=1.9$ and $\alpha=0.10$. Note that the exponent is zero to within numerical accuracy when the attractor takes the form of a set of closed, smooth curves around which the orbit circulates.

Hénon map; see Fig. 5). However, the transition that begins at $\epsilon\approx 0.339$ in Fig. 10 (and that at $\epsilon\approx 0.25$ in Fig. 12) is very different. This second bifurcation sequence begins when a set of periodic points lose stability in a Hopf bifurcation and loopy attractors appear; we delve further into the structure of this sequence in Sec. VI C.

There are also numerous transitions in which one attractor suddenly disappears, leaving a different one. Several of these transitions occur through a saddle-node or subcritical bifurcation. In other cases, an attractor is annihilated on collision with an unstable object (a ''crisis''). For example, the bifurcation sequence terminates to the right in Fig. 10 ($\epsilon\approx 0.425$) as a result of a saddle-node bifurcation of a period-6 orbit. In Fig. 10, there are also two subcritical bifurcations that destabilize the period-3 solution and create the chaotic window over the range 0.40–0.41. The transition to the left of this picture at $\epsilon\approx 0.32$ occurs as a result of a collision. These types of transitions terminate the more compact, asynchronous attractors at the lowest and highest values of ϵ in all the cases we considered.

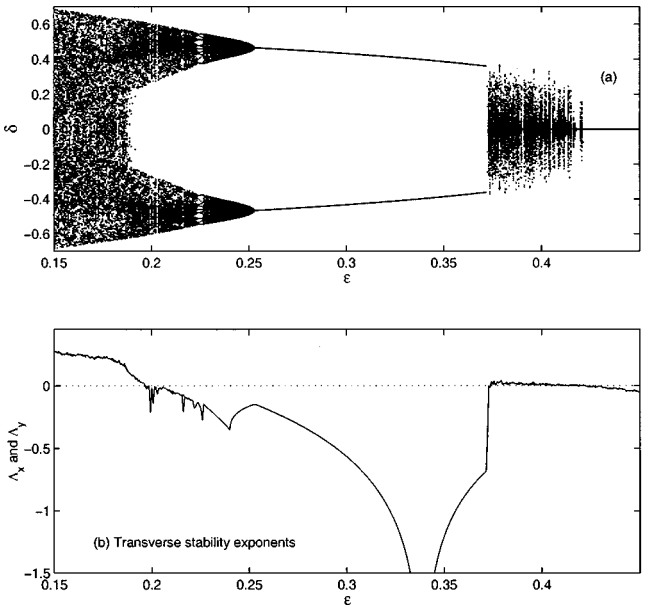

FIG. 12. Bifurcation diagram for the two-family map with $a=1.9$ and $\alpha=0.50$. (a) δ_n, (b) the transverse stability exponents, Λ_x and Λ_y. This two-family solution is equally partitioned and so must be symmetrical in X and Y; any differences in Λ_x and Λ_y are purely a result of poor convergence (none are evident in the picture).

One feature of the rightmost transition is that if it occurs for sufficiently large ϵ, no attractors apparently remain other than the synchronized state. But when $\epsilon<\epsilon_c(1.9)\approx 0.42$, this state is unstable. If the original attractor disappears when $\epsilon<\epsilon_c$, this leads to solutions for which there is a substantial amount of intermittent bursting off the synchronized state. This is a form of on–off intermittency and was previously explored in Refs. 4 and 5. The intermittent bursts produce the unusual structure to the bifurcation diagram in Fig. 11 over the range 0.41–0.43.

Another curious feature of the bifurcation diagrams in Figs. 10 and 11 is the preponderance of period-3 orbits and their subharmonics. However, this is purely a property of maps with parameters $a=1.9$ and small α, and is coincidental. For example, the bifurcation diagram shown in Fig. 12 for the equally partitioned two-family map is dominated by a period-2 orbit. That period-2 orbit is the same as that whose stability is shaded in Fig. 1.

C. Break-up of loopy attractors

The bifurcation sequence beginning at $\epsilon\approx 0.339$ in Fig. 10, and shown in more detail in Fig. 13, is initiated when a period-3 orbit loses stability in a Hopf bifurcation. A similar transition takes place for the period-2 orbit in Fig. 12. In the bifurcation, a limit cycle is shed about each point of the

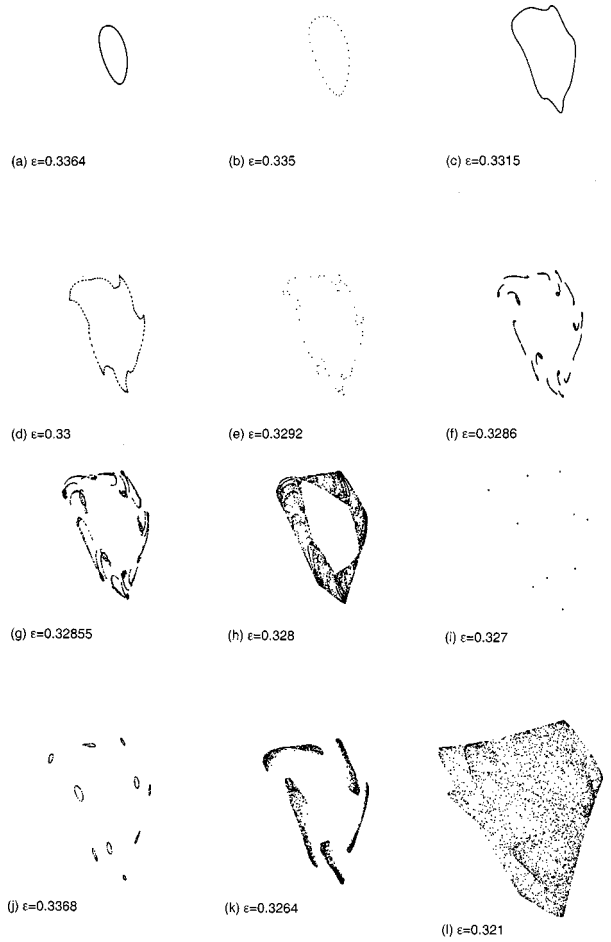

FIG. 14. Pictures of parts of the developing attractor on the (X_n, Y_n) plane for $\alpha = 0.10$ and various values of ϵ between 0.336 and 0.32.

periodic orbit [Fig. 14(a) shows one such loop]. On lowering ϵ further, the attractor develops and passes through a sequence of more bifurcations (see Fig. 14). This sequence is similar to ones presented in.[19–22]

Superficially, the sequence has two distinct types of bifurcations. First, the attractor passes through a succession of bifurcations in which the loops disintegrate into sets of periodic points. These points persist for a while but eventually disappear, leaving another curve [see Figs. 14(b) and 14(c); this creates the ''band'' near $\epsilon = 0.331$ in Fig. 13]. This is a phase-locking transition that is familiar from circle maps. In fact, when the attractor of the two-dimensional map takes the form of a closed curve around which the orbit circulates, then the dynamics on this attractor is exactly a circle map.

To make this reduction more apparent, we take the closed loops of the attractor shown in Figs. 14(a), 14(b), and 14(d) and use an angular coordinate, θ_n, to parameterize the curves. The first return map of this variable is shown in Fig. 15. For the final attractor, the parametrization by θ is multivalued and the return map is consequently not quite one dimensional.

The second type of transformation shown by the developing attractor is in the shape of the curve itself. Just beyond the initial bifurcation, the attractor is a set of simple loops. But as ϵ decreases the curve of the attractor appears to develop a nonsmooth structure wherein several ''kinks'' emerge in the loop. A parametrization of the attractor would at this stage be nonanalytic. An attractor just beyond this transition is shown in Fig. 16; at smaller ϵ still, the geometry of the object is even more complex and individual curves are no longer distinguishable [Fig. 14(f)–14(i)].

It is at this stage of the bifurcation sequence that the attractor first becomes chaotic (we verify this using the leading Lyapunov exponent of the attractor as shown in Fig. 13), and the object in Fig. 16 looks to have fractal structure. This inception of chaos seems intimately connected with the change in the structure of the curve of the attractor; there was no situation in which points chaotically iterated around a smooth curve. In fact, the transition probably follows the route to chaos by way of a strange, nonchaotic attractor.[23–25]

D. Transverse stability

Transverse stability is determined by the statistical averages in (24). In Figs. 10–12, we also include panels showing the transverse stability exponents; for values of ϵ where at least one of these is positive, the ''attractors'' are unstable in the full lattice system.

In the bifurcation diagrams 10–12, there are several ranges over which the states lose transverse stability. Notably, the states always become unstable at sufficiently small ϵ. Sometimes, this instability sets in at the point of crisis of a relatively compact attractor ($\epsilon \approx 0.32$ in Fig. 10, $\epsilon \approx 0.322$ in Fig. 11). Beyond that point, the attractor suddenly expands to fill a much larger expanse of the phase space, and consequently the average of $\ln X_n$ or $\ln Y_n$ changes discontinuously.

However, the sudden expansion of the attractor does not always coincide with the point of transverse instability. For example, in Fig. 12, transverse stability apparently disappears at $\epsilon \approx 0.195$ where the attractor is still relatively com-

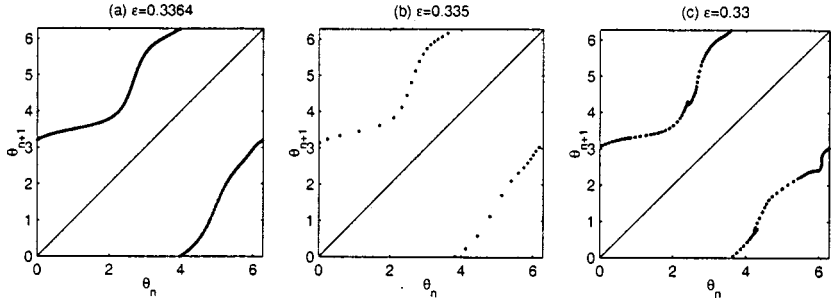

FIG. 15. Maps derived by taking the attractors of Figs. 14(a), 14(b), and 14(d), parameterizing the curves by an angular coordinate, θ_n, and then plotting θ_n against θ_{n+1}.

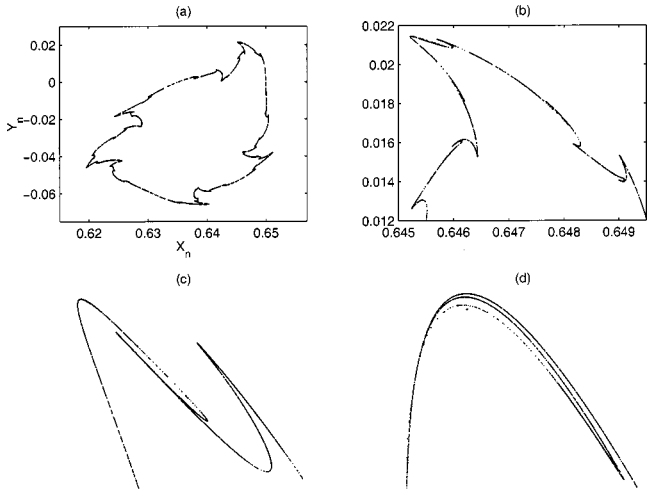

FIG. 16. Fractal attractor on the (X_n, Y_n) plane for $\epsilon = 0.329\,215$, $\alpha = 0.1$, and $a = 1.9$. The panels show successive magnifications of the uppermost tip of the object.

pact. In Fig. 11, on the other hand, the attractor remains transversely stable down to about $\epsilon = 0.365$, whereas crisis occurs at $\epsilon \approx 0.37$.

In spite of these minor distinctions, it remains generally the case that on the full lattice, compact attractors of the two-family map are more stable than extensive ones. Moreover, when extensive attractors are transversely stable (such as over the approximate range 0.40–0.41 in Fig. 10), their stability exponents are significantly smaller in magnitude than those of compact attractors. This suggests that the basins of attraction of compact attractors might be larger than

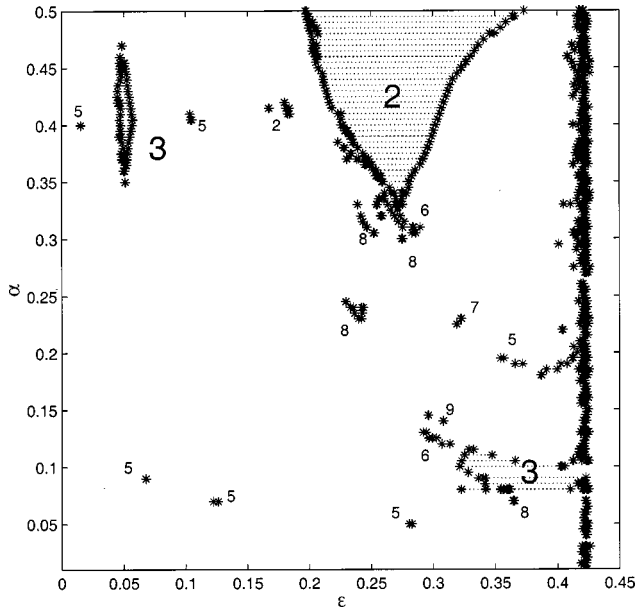

FIG. 17. Ranges over which two-family solutions are transversely stable, plotted on the (ϵ,α) plane. $a = 1.9$ and $N = 200$. The numeric labels give a rough idea of the number of distinct pieces in the attractor. The computations were performed by taking initial conditions from the final state of the computation at the previous value of ϵ and iterating 10^4 times; there is no attempt to account for multiple attractors. Fuzzy borders reflect either irregular functional dependence on parameters, or poor numerical convergence.

those of extensive attractors in the phase space of the full lattice system. Hence, because the compact attractors are typically periodic, the two-family states that one should observe in the full lattice system at $a = 1.9$ ought to be on the whole periodic. This is a feature brought out in the initial-value computations of Sec. V (see Table II). Reasons why partitioned states are often periodic are given by Shinbrot[26] and Parravano and Cosenza.[27]

More details on the phenomenology of two-family states on the full lattice can be gleaned from Fig. 17, which shows the ranges in ϵ over which attractors of two-family maps with different partitions are transversely stable. From this stability diagram, it is clear that the two-family states lie over two characteristic ranges in ϵ. At larger coupling strengths, states with relatively unbalanced partitions should predominate with a basic period of 3. At smaller ϵ, more balanced partitions should emerge, with a base period of 2. There is also a narrow strip near $\epsilon = 0.4$ in which there appear to be transversely stable, chaotic bursters, and a narrow island of period-3 solutions at $\epsilon \approx 0.05$. [These solutions have very slowly converging statistical properties due to the highly intermittent dynamics, and so the transverse stability exponents are not well determined. For the same reason, the analogous results of the initial-value computations shown in Fig. 8(b) are also not completely definitive.] This picture rationalizes completely the results of the initial-value computations shown in Fig. 8b. In addition, the more refined computations uncover more two-family attractors existing in small regions scattered over the (ϵ,α) plane.

For some of the transitions to transverse instability, both of the exponents pass through zero simultaneously (this is typical of a crisis-induced transition, e.g., $\epsilon \approx 0.322$ in Fig. 11). But in other situations, only one of these exponents becomes positive (e.g., $\epsilon \approx 0.36$ in Fig. 11). In this latter case, because of the structure of the transverse stability eigenvectors, only one of the synchronized families is unstable to low-amplitude perturbations. As a consequence, the instability can destroy the synchrony of that family, but leave the other partition intact. This leads to a novel kind of bifurcation in which one of the partitions fragments into further families. That is, K-family to K'-family transitions.

A two-family to three-family transition is shown in Fig. 18. In this example, a chaotic state with $\alpha = 0.35$ lost stability to perturbations that fragmented the partition containing 65 maps. A periodic, three-family state resulted with partition (35, 31, 34). It is this type of transition that is probably behind the feature displayed in Fig. 8, that the domain of the $K = 3$ attractors appears to be an extension of the triangular region in which two-family attractors reside.

Such bifurcations may occur in both periodic or chaotic states. In the latter case, the transition can lead to prolonged bursting, much as the loss of stability of the synchronized state leads to on/off intermittency. In fact, this effect probably lies at the heart of the ephemeral states observed in the transients mentioned in Sec. V (see Fig. 4). Also, each bifurcation is highly degenerate, and there are many multiple solution branches that are born at these points. As a result, after the inception of one of these instabilities, the possible final lattice states can be very varied, ranging from simply struc-

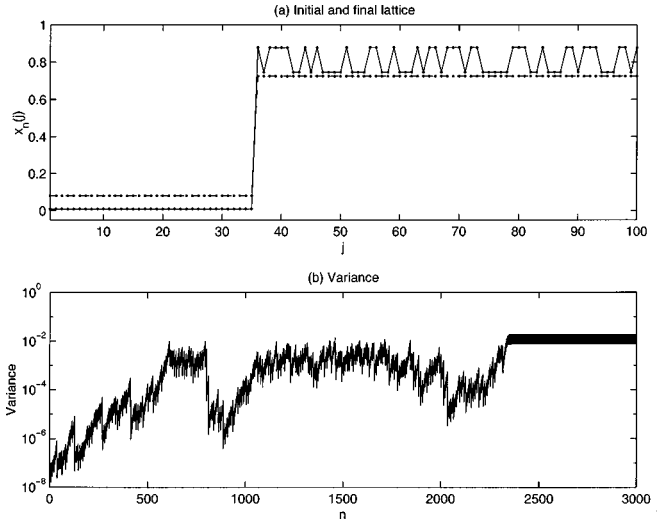

FIG. 18. Generation of a three-family state from a slightly unstable two-family solution. (a) The initial (dashed line) and final (solid line) lattices. (b) The variance in the values of $x_n(j)$ for the original second family displayed against n.

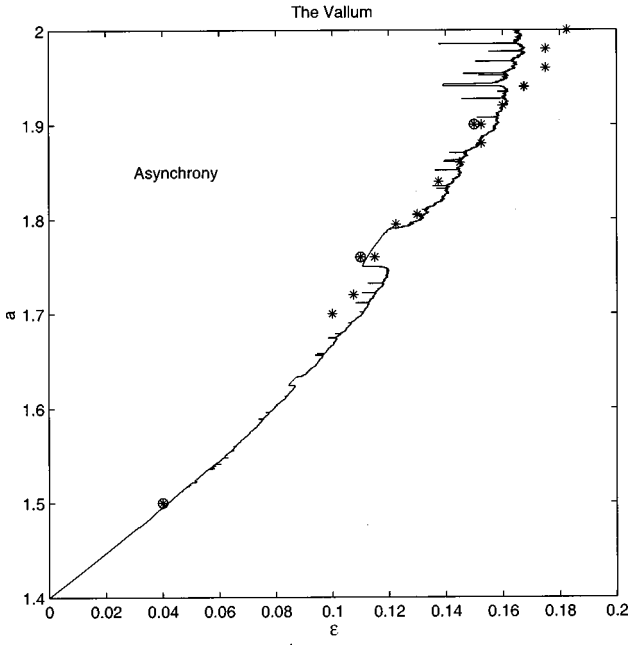

FIG. 19. The location of the desynchronization cliff. The stars indicate empirical estimates based on the initial-value computations also shown in Fig. 6. The circled stars denote measurements based on the parameter slices of Sec. V A.

tured fragments to complicated ones, and from periodic to chaotic lattices.

VII. CONCLUSION

In this work, we have explored the dynamics of a lattice of globally coupled logistic maps. Below the threshold of full synchronization, a complicated behavior emerges.

When the individual maps are in a periodic regime, and at small coupling strength, we observe coexistence of an enormous number of attractors. Here, then, the complexity of the lattice dynamics far exceeds that of the individual elements; the whole is, in fact, greater than the sum of the parts.

An extensive set of initial-value calculations at larger map parameter has indicated that the system often organizes itself into multiple, synchronized families. This organization produces periodic or weakly chaotic lattices over a large portion of parameter space in which the individual maps of the lattice would otherwise be chaotic. In our opinion, one of the most interesting aspects of the dynamics of globally coupled maps is this apparent suppression of chaotic behavior. Of the partitioned solutions, the two-family solution is particularly important as it is frequently observed. For this reason, we have studied in detail the dynamics of two-family solutions.

Many of our results are concisely summarized in Fig. 1; this picture displays the most interesting portion of the parameter plane (coupling strength against map parameter). The cliff is one of the most remarkable features in Fig. 1. Roughly speaking, one can regard it as the beginning of true asynchrony on the lattice. This is not completely accurate, of course, because robust synchronized states do appear at isolated parameter values beyond the cliff [these are the ''pockets'' of synchrony that reappear at small ϵ in Fig. 7(b)]. Moreover, such states can be important to the statistical mechanics of the lattice at weak coupling (see Refs. 7 and 28). However, broadly speaking, lattices are incoherent beyond the cliff.

We can find an approximate location of the cliff by considering asynchronous lattices in the limit $N\to\infty$. Here, the mean field is

$$M_n = 1 - \frac{1}{N} a \sum_{j=1}^{N} [x_n(j)]^2, \tag{25}$$

but when the elements of the lattice are incoherent, the average over the lattice is equivalent to an average over possible realizations of each element. That is, the average in (25) can be replaced by a statistical average over each (identical) attractor, $\Phi = \langle x^2 \rangle$. Thus each map evolves according to

$$x_{n+1} = (1 - a x_n^2)(1-\epsilon) + \epsilon(1 - a\Phi) \tag{26}$$

(cf. Refs. 29 and 30). Equation (26) is not as simple as it seems because the constant Φ itself depends on the statistical properties of the attractor which are not known *a priori*.

We may recast Eq. (26) into the form of the logistic map by a simple transformation:

$$\zeta_{n+1} = 1 - \tilde{a}\zeta_n^2, \quad \zeta_n = x_n/(1-\epsilon a\Phi) \tag{27}$$

and

$$\tilde{a} = (1-\epsilon a\Phi)(1-\epsilon)a. \tag{28}$$

Evidently, the ''effective'' value of the map parameter is reduced by the collective effect of the incoherent lattice, which epitomizes how the coupled map lattice is now more regular than its individual elements (the whole is less than the parts).

However, to be incoherent, the elements must all be chaotic, and so $\tilde{a} > a_\infty$. Hence,

$$(1-\epsilon)(1-\epsilon a\Phi)a > a_\infty; \tag{29}$$

or,

$$\epsilon < \epsilon_V = \frac{(1+a\Phi) - \sqrt{(1+a\Phi)^2 + 4a_\infty \Phi}}{2a\Phi}. \tag{30}$$

In other words, $\epsilon = \epsilon_V$ is the border of asynchrony, the cliff.

We compare empirical estimates of the location of the cliff with the prediction (30) in Fig. 19. However, in order to simplify the computation, we approximate $\Phi = \langle x^2 \rangle$ by its value for $\epsilon = 0$; that is, by the corresponding value for the logistic map. The approximate prediction and the empirical data agree surprisingly well. Note that the windows of stable periodic orbits of the logistic map appear in Fig. 19 as leftward excursions of the approximate prediction (for example, the period-3 window is evident over the range in a, [1.76, 1.79]). Because such orbits cannot be incoherent on the lattice, the approximation does not provide a value of Φ that can be trusted over these ranges. However, the average of the true attractor is not likely to be very different.

Several questions remain to be answered. For example, it would be interesting to study the behavior of a ''passive map;'' that is, a map which is influenced by the others but does not feed back on the lattice (cf. Refs. 26 and 27). This may provide a first step toward a mean field theory of globally coupled maps.[31] Another intriguing question that is left open is what is the fate of the complexity observed here when the coupling becomes local, and lattice sites acquire a truly spatial meaning. Another issue that may be relevant in a variety of applications focuses on the dynamics of maps that are subject to an external forcing field. We hope to address some of these issues in future works.

ACKNOWLEDGMENTS

This research was initiated at the 1998 Geophysical Fluid Dynamics Summer Study Program, Woods Hole Oceanographic Institution, which is supported by the N.S.F. and O.N.R. We thank the ISI Foundation, Torino, for hospitality during part of this work.

[1] K. Kaneko, ''Overview of coupled map lattices,'' Chaos **2**, 279 (1992).
[2] *Theory and Applications of Coupled Map Lattices, Nonlinear Science: Theory and Applications*, edited by K. Kaneko (Wiley, West Sussex, 1993).
[3] K. Weisenfeld and P. Hadley, ''Attractor crowding in oscillator arrays,'' Phys. Rev. Lett. **62**, 1335 (1989).
[4] Q. Zhilin and G. Hu, ''Spatiotemporally periodic states, periodic windows, and intermittency in coupled-map lattices,'' Phys. Rev. E **49**, 1099 (1994).
[5] M. Ding and W. Yang, ''Stability of synchronous chaos and on–off intermittency in coupled map lattices,'' Phys. Rev. E **56**, 4009 (1997).
[6] K. Kaneko, ''Chaotic but regular posi-nega switch among coded attractors by cluster-size variation,'' Phys. Rev. Lett. **63**, 219 (1989).
[7] K. Kaneko, ''Clustering, coding switching, hierarchical ordering, and control in a network of chaotic elements,'' Physica D **41**, 137 (1990).
[8] K. Kaneko, ''Relevance of dynamical clustering to biological networks,'' Physica D **75**, 55 (1994).
[9] L. Fabiny and J. Weisenfeld, ''Clustering behavior of oscillator arrays,'' Phys. Rev. A **43**, 2640 (1991).
[10] D. Golomb, D. Hansel, B. Shraiman, and H. Sompolinsky, ''Clustering in globally coupled phase oscillators,'' Phys. Rev. A **45**, 3516 (1992).
[11] D. H. Zanette and A. S. Mikhailov, ''Condensation in globally coupled populations of chaotic dynamical systems,'' Phys. Rev. E **57**, 276 (1998).
[12] M. G. R. A. S. Pikovsky and J. Kurths, ''Synchronization in a population of globally coupled chaotic oscillators,'' Europhys. Lett. **34**, 165 (1996).
[13] R. S. MacKay and S. Aubry, ''Proof of existence of breathers for time-reversible or Hamiltonian networks of weakly coupled oscillators,'' Nonlinearity **7**, 1623 (1994).
[14] F. Xie and G. Hu, ''Clustering dynamics in globally coupled map lattices,'' Phys. Rev. E **56**, 1567 (1992).
[15] M. Cencini, M. Falcioni, D. Vergni, and A. Vulpiani, ''Macroscopic chaos in globally coupled maps'' (unpublished).
[16] K. Kaneko, ''Partition complexity in a network of chaotic elements,'' J. Phys. A **24**, 2107 (1991).
[17] K. Kaneko, ''On the strength of attractors in a high-dimensional system: Milnor attractor network, robust global attraction and noise-induced selection,'' Physica D **124**, 308 (1998).
[18] A. Csilling, I. M. Janosi, G. Pasztor, and I. Scheuring, ''Absence of chaos in a self-organized critical coupled map lattice,'' Phys. Rev. E **50**, 1083 (1994).
[19] A. Arnéodo, P. Coullet, and E. A. Spiegel, ''Cascade of period-doublings of tori,'' Phys. Lett. **94**, 1 (1983).
[20] K. Kaneko, ''Oscillation and doubling of torus,'' Prog. Theor. Phys. **72**, 202 (1984).
[21] K. Kaneko, ''Fractalization of torus,'' Prog. Theor. Phys. **71**, 1112 (1984).
[22] V. Franceschini and C. Tebaldi, ''Breaking and disappearance of tori,'' Commun. Math. Phys. **94**, 317 (1984).
[23] C. G. M. Ding and E. Ott, ''Evolution of attractors in quasiperiodically forced systems: From quasiperiodic to strange nonchaotic to chaotic,'' Phys. Rev. A **39**, 2593 (1989).
[24] A. S. Pikovsky and U. Feudel, ''Characterizing strange nonchaotic attractors,'' Chaos **5**, 253 (1995).
[25] T. Nishikawa and K. Kaneko, ''Fractalization of a torus revisited as a strange nonchaotic attractor,'' Phys. Rev. E **54**, 6114 (1996).
[26] T. Shinbrot, ''Synchronization of coupled maps and stable windows,'' Phys. Rev. E **50**, 3230 (1994).
[27] A. Parravano and M. G. Cosenza, ''Driven maps and the emergence of ordered collective behaviour in globally coupled maps,'' Phys. Rev. E **58**, 1665 (1998).
[28] A. S. Pikovsky and J. Kurths, ''Do globally coupled maps really violate the law of large numbers?'' Phys. Rev. Lett. **72**, 1644 (1994).
[29] K. Kaneko, ''Globally coupled chaos violates the law of large numbers but not the central-limit theorem,'' Phys. Rev. Lett. **65**, 1391 (1990).
[30] T. Shibata and K. Kaneko, ''On the tongue-like bifurcation structures of the mean-field dynamics in a network of chaotic elements,'' Physica D **124**, 163 (1998).
[31] K. Kaneko, ''Remarks on the mean field dynamics for coupled maps,'' Physica D **86**, 158 (1995).